Bulletin de la Socié Royale des Sciences de Liège - Vol. 74, 1-2-3, 2005, pp. 1-16

Basic and future concepts of interferometers, including the confusion effect

P. Riaud [1], S. Cladé [2], O. Absil [1], L. Arnold [3]

[1]Institut d'Astrophysique et de Géophysique, Université de Liège, Belgique
[2]Service d'Aéronomie du CNRS, Verrière le Buisson, France
[3]Observatoire de Haute-Provence, France

Abstract: In this paper, we discuss the different recombination techniques in stellar interferometry and their implications in imaging reconstruction. Actually, three techniques exist for imaging interferometers : Fizeau, Densified and IRAN, each with different interests. Because of an incomplete frequency coverage in the (u,v) plane, all interferometers give a poor image quality with multiple bright peaks in direct imaging. This effect decreases the detectivity of faint sources due to the crowding effect. The aim of this article is to investigate this confusion problem in the both cases of a single pupil and of an interferometric array. Confusion noise is the crowding effect between the different sources present in the field of view of the instrument. This effect becomes important when the instrument has a large collecting surface and a weak quality for its Point Spread Function. This study gives an estimation of detectivity loss due to confusion noise with the different optical instruments.

1 Introduction

Since the beginning of the century, optical interferometry has significantly improved. After some hesitation, the VLTI has emerged with a complete useful observing interface entering the scientific era of interferometry for the ESO community. Now, many propositions are made to upgrade the instrumentation to perform deeper exploration of the universe and to achieve higher resolution. Two architectures are in competition: the Extremely Large Telescopes like OWL, and various very long baseline interferometric arrays (up to ten kilometers) with a large number of sub-apertures. The aim of this article is to discuss one of the main limitation of both architectures: confusion noise. First, we introduce and discuss the theory of interferometric recombination process. Secondly, we simulate the imaging properties for two examples (one in each architecture) under realistic atmospheric turbulence assumptions. Finally, we show the effect of residues in the halo due to diffraction effects or partial correction of turbulence on the detectivity of faint sources. In the conclusion, we discuss the possible optimization of instruments regarding the limitation of confusion noise.

2 Principle of interferometry

This chapter discusses the properties of diffraction processes for a single pupil instrument and for interferometers. We will see afterwards how to separate astrophysical effects from instrumental effects and how to optimize instruments. It is interesting to start the study of diffraction processes for interferometers by first considering the case of a single telescope or aperture. Let us return to propagation of light in the optical instruments. In all light beams, some energy is spread outside the region predicted by rectilinear propagation. This effect, known as diffraction, is fundamental and explains all image properties in the optical instruments.

Diffraction can be understood by considering the wave nature of light. Huygens's principle states that each point on a propagating wavefront is an emitter of secondary wavelets. The combined locus of these expanding wavelets forms the propagating wave. Interference between the secondary wavelets gives rise to a fringe pattern that rapidly decreases in intensity with the increase of the angle from the initial direction of propagation. Huygens's principle nicely describes diffraction, but rigorous explanation demands a detailed study of wave theory. In this case, the diffraction theory is given by the Huygens's integral but this mathematical assumption is not usable easily for simple instruments like telescopes.

The first order development by the Fresnel propagation integrals gives a good approximation of images properties in most optical devices including astronomical devices like telescopes. The Fresnel diffraction primarily concerns what happens to light in the immediate neighborhood of a diffracting object or aperture. It is thus only of concern when the illumination source is close to this aperture or object.
If the object source is at a quasi-infinite distance, e.g. a star, the aperture (telescope or interferometer) is illuminated by a plane-wave. The diffraction process can be calculated by a simple Fourier transform of the instrument pupil. This is the Fraunhofer diffraction, which determines the limiting performance of optical systems. The Fourier analysis determines the frequency distribution of the object observed through the optical instrument considered. In fact, an ideal single telescope without central obscuration samples the observed object at all frequencies under the cut-off frequency, determined by the finite size of the instrument. We conventionally denote the frequency coordinates by u,v (units of fringe cycles per radian on the sky with interferometric architecture). This base will be important in all recombination process to reconstruct images. Indeed, the classical circular pupil gives, through a Fourier transform, the Airy pattern (Bessel function of the first kind - $J_1(r)^2/r^2$) as an impulse response. This impulse response is conveniently designed by Point Spread Function (PSF hereafter). The diffraction effect determines directly the resolution performance.

The response of the optical instrument to extended objects is related to the Fourier transform of the object brightness distribution under certain assumptions (source incoherence and small-field approximation). This relation is known as the van Cittert-Zernike theorem. The convolution theorem gives directly the observed image by the convolution of the object with the PSF. We will see later that for densified recombination this theorem is not directly applicable. It is relatively simple to describe an interferometer as an instrument having the same resolution performance than a single pupil with a diameter of B, with B the baseline of the interferometer, but a limited frequency coverage. We consider astronomical interferometers because they provide access to high angular resolution at a small fraction of the price of an equivalent single pupil.

The first idea to use an interferometer for stellar diameter measurement was developed by H. Fizeau and E. Stephan in 1868 at Marseille Observatory with 80 cm reflector. A few years later, A. Michelson observed Galilean satellites with a larger baseline. In 1920, A. Michelson built a large (7 meters long) steel beam with two plane mirrors of small diameter at Mt Wilson on the 100 inch telescope (Michelson & Pearse 1920). He measured the diameter of the star Betelgeuse by fringe contrast measurement. Indeed, when the source is resolved by the baseline of the instrument, the contrast decreases due to the convolution effect of the object size on the Point Spread Function.

2.1 The recombination process

We will see in this chapter the different recombination processes for direct imaging. There are three different manners to recombine separated telescopes. Figure 1 shows in those three cases the focal plane of an interferometer composed of five telescopes.

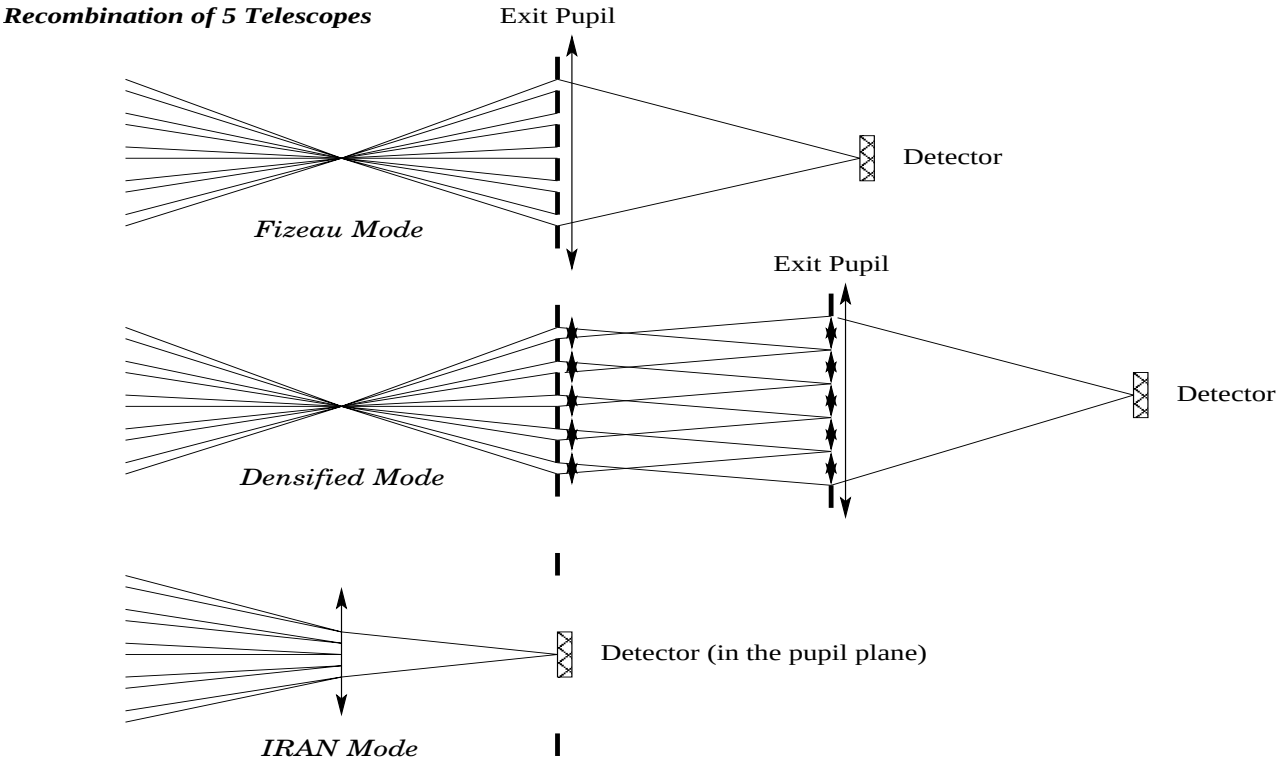

Figure 1: These are the three different recombination modes. Top: The Fizeau mode where the proportion of the sub-pupils sizes and spacings remains unchanged. Middle: The densified mode where an appropriate optical setup increases the relative size of the sub-pupils in the final exit pupil of the full interferometric array. Bottom: The IRAN mode: the different images (amplitudes) of each telescopes are recombined, forming an interferometric image in the pupil plane.

2.1.1 The Fizeau Mode

This first recombination method was developed by Hippolyte Fizeau in 1868 (Fizeau 1868, Roddier F. & Ridgway S.T., 1999).It consists in making direct homodyne combination of sub-apertures without size change (in proportion) for each sub-pupil. In this condition, the diameter

ratio between the sub-apertures and the baseline is preserved from the entrance to the exit pupil of the system. This recombination corresponds, in the image plane, to the multiplication of the telescope impulse response (diffraction of each sub-aperture) with the interferometric pattern (the Fourier transform of the Dirac distribution corresponding to the position of each sub-aperture). The result is a fine fringe pattern due to the interference between telescopes, modulated by a large diffraction disk. Figure 3 shows a Fizeau recombination with 37 telescopes. If the shape of the sub-apertures is not circular, the modulation function is not a simple Airy pattern but a function that takes into account the shape of the pupil. This function is numerically calculable for all shapes like for example squares or hexagons.
This architecture has the interesting property to allow a wide elementary field of view, only limited by the diameter of the first ring of the Airy pattern. A large number of elementary field are possible in multi-field imaging devices. In the case of large dilution factor (small diameter of sub-apertures and long baselines), the focal plane image features one white fringe and many (hundred or more) dispersed fringes. Only a fraction of the energy is in the white fringe, so that the signal to noise ratio decreases quickly as the square of the dilution factor ($\approx (B/d)^2$, with B the baseline of the interferometer and d the diameter of the sub-apertures).

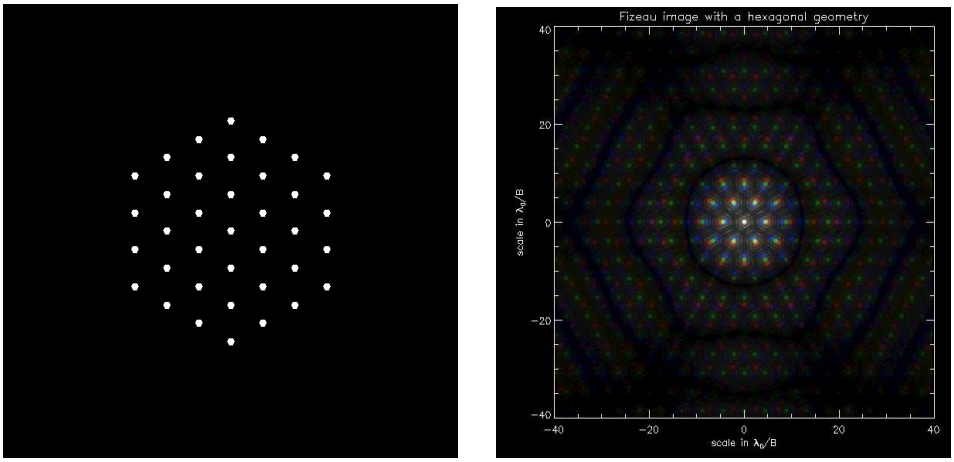

Figure 2: Fizeau recombination with 37 telescopes in a hexagonal arrangement. Left: entrance and exit pupil configuration, with a dilution factor $\gamma = B/d = 32$. Right: focal plane image for a point like source with a spectral bandwidth of 5. The wavelength is centered at $2.2\mu m$ (the K band) and the Strehl ratio is 100% (perfect case).

It is possible to increase the signal to noise ratio in Fizeau mode by adding to the white peak the contribution of the dispersed peaks, using a photon counting camera. But this process is limited by the readout noise of classical cameras. Indeed, we can sum all the peaks having a signal to noise ratio larger than 3σ. The signal to noise ratio increases only by a factor lower than the square root of number peaks.

2.1.2 The Densified Mode

The Fizeau technique produces multiple interference fringes for a point like source. It is possible to obtain in the image plane only one fringe per source using densified or generalized Michelson recombination. Indeed Michelson used a different recombination than the classical Fizeau in experiment at Mont Wilson (Michelson & Pease 1921): the two entrance pupils have

been separated by a baseline of 7 meters, and with two plane mirrors, he artificially joined the two pupils. This is the same as to increase with a simple homothety the sub-aperture sizes in the exit pupil. In 1996, Antoine Labeyrie proposed to use this technique in the case of N sub-apertures (Labeyrie 1996).
If we choose a sufficiently redundant configuration, we obtain a monolithic exit pupil after the densification process. This principle generalizes the classical Michelson interferometer for N telescopes. This technique is usable when the sub-apertures are similar in shape. If not, we can anamorphose the sub-pupils. The extreme example is given by the PIAA (Guyon 2003) with the use of a continous densification. The most interesting property of the densified image is the intensification of the white peak. Indeed all the dispersed peaks previously present in the Fizeau image disappear and by energy conservation these contributions are restored in the white peak. The technique reduces the field of view to a small not aliased field of view. For the sake of clarity, we will define two different fields of view for densified and Fizeau interferometers. First of all, we define the Zero Order Field (ZOF hereafter), where all polychromatic images are concentrated in one "white" peak . It corresponds to the zero order of classical gratings in spectroscopy. This field of view is narrow. Its size depends on three parameters: the number of sub-apertures, the dilution factor and the redundancy of the interferometric architecture.
Secondly, we define the High Order Field (HOF hereafter). It correponds to the wide field of view of the Fizeau mode limited by the diameter of the first ring of Airy pattern associated to a sub-aperture. This field of view can be relatively "large", i.e. about 0.6" to 3" for an Auxiliary Telescope at VLTI in K to M bands.
In this configuration, all sources present in the HOF form a dispersed image in the ZOF. If the sources are already in the ZOF, they gives one "white" peak per sources. On the other hand all sources in the HOF give dispersed and intensified peaks in the ZOF. According to the densified configuration with 37 telescopes, we can have a maximum of three dispersed peaks in the ZOF. An important effect of densified pupil, concerning mathematical aspect, is the loss of the convolution relation between the object and the final image, because the HOF field of view is now concentrated in the narrow field of view (ZOF).

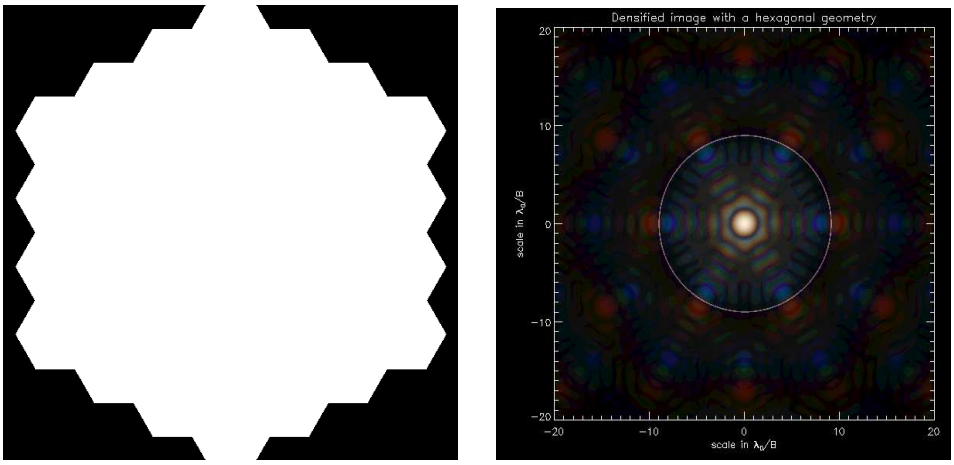

Figure 3: Densified recombination with 37 telescopes (hexagonal shape). Left: We only show the exit pupil configuration, because the entrance pupil is the same as the previous Fizeau configuration. Right: focal plane image for a point like source with a spectral bandwidth of 5. The spectral bandwith is centered at $2.2\mu m$ (the K band) and the Strehl ratio is 100% (perfect case). The dashed circle defines the limit of the Zero Order Field (ZOF).

2.1.3 The Iran Mode

The "IRAN" mode is the last recombination mode usable in direct imaging interferometry. This mode is slightly different from the previous ones, because the partial densification recombination happens in the focal plane and not in the pupil plane. The result is a densified image in the pupil plane. It is thus necessary to reverse our way of thinking the imaging process. This mode was proposed after the densification idea, by Vakili et al. 2004.
The technique consists in approaching the different amplitudes collected by each sub-aperture to form a very dense unit in the focal plane (see Fig 4a.). In the relayed pupil (after a Fourier Transform), a set of narrow peaks is formed with faint rings like classical Airy patterns. The author call Point-Source Intensity Distribution (PSID) this image formed in the pupil plane. It is indeed different from a Point Spread Function. This "image" in the pupil plane corresponds to the convolution of the Dirac peaks (the positions of each image in the focal plane provided by the telescopes) with a gate function.
This technique allows a partial recombination to avoid crowding effects between Airy rings but the gain factor in the peak is lower than for the classical densification proposed by Labeyrie. The main advantage of IRAN is to keep the convolution relationship between object and final image. But the gate function limitates the total field of view to the exit pupil and does not allow multiple field imaging capabilities such as densified imaging (see the chapter on confusion effect). However, in spite of the fact that we form an image in the pupil plane, the field of view usable with this technique is the same as the ZOF defined in densified imaging. Indeed, beyond the ZOF, the recombination creates multiple peaks that limitate the scientific applications.
Note that the convolution relationship is kept if the sub-aperture PSFs are anamorphosed properly (see Fig. 4). This obligation seems however difficult to realize in an optical workbench.

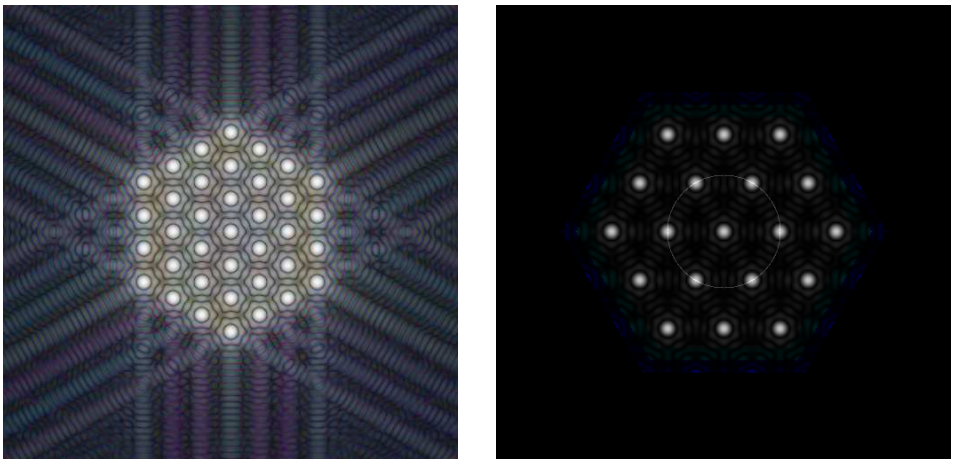

Figure 4: IRAN recombination with 37 telescopes (hexagonal shape). Left: focal plane configuration with a spectral bandwidth of 5. Right: image in the pupil plane for a point like source. The wavelength is centered at $2.2\mu m$ (the K band) and the Strehl ratio is 100% (perfect case). The circle defines the limit of the Zero Order Field (ZOF) applicable to IRAN recombination.

We will come back more precisely on the field of view properties of interferometers when discussing confusion problems.

3 The confusion problem

The problem of confusion, i.e., the crowding of the different sources in the observed field of view, is rarely studied in optical instruments. Indeed, this type of study asks for a strong interaction between optical design and scientific issues. An example of strong constraints for optical instrumentation is the case of high contrast imaging with coronagraphy. The detection of a planet around a nearby star [1] with a coronagraph needs an optimization of the full optical design, especially the optical wavefront errors, and also raises the possibility to use an off-axis telescope to avoid the central obscuration that is harmful for most coronagraphic devices. In this case, the confusion problem directly depends on the optical architecture: single pupil or interferometer.
The confusion problem with a classical telescope (single aperture) is directly related to the PSF extension. For a perfect telescope without central obscuration, the Airy pattern decreases in θ^{-3} where θ is the angular resolution. At $\theta = 10\lambda/d$ the PSF intensity is still 3×10^{-5} of the central peak. The source crowding corresponds to the convolution process of the observed sources with the PSF. In the case of interferometric confusion the effect is double: the convolution process (as for a single pupil) and also the limited field of view of the instrument (the Zero Order Field previously defined). Generally, an interferometric instrument has a lower detectivity than a single pupil.
In this paper, we estimate the loss in detectivity for these two architectures.

4 Simulation results

Let us first present the input atmospheric constraints (Roddier 1987) with extreme adaptive optics corrections. We use a simplified model of AO: only one layer of turbulence and the properties of the corrected phase screen given by a simple PSD (Power Spectral Density). A simulation with three layers of turbulence is computing time demanding and shows only little difference with this simplified model. For real observations, the use of an MCAO [2] architecture to correct the wavefront bumpiness on a larger field of view (typically $2' \times 2'$) taking into account the three different layers of turbulence may improve the result. In our case, we use a simplified model with the parameters listed in Table 1.

The numerical simulations are performed with large arrays (4096×4096) to limit the aliasing effect associated to the FFT algorithm and to allow sufficient focal plane sampling (5 pixel / resel [3]). Finally, 1024 speckle realizations are added at nine different wavelengths to provide a polychromatic PSF for a simulated long exposure time.

We will take the same parameters for interferometer simulations and also keep the same sampling for the number of actuators (16 actuators per square meter).

[1] the contrast between the star and the planet can reach 10^{10} for a terrestrial planet in the visible
[2] Multi-Conjugate Adaptive Optics
[3] 1 resel = $(\lambda/d)^2$ for a single pupil or $(\lambda/B)^2$ for an interferometer

Seeing @ 0.55 μm	0.8"
Wind speed	15 m/s
D/r_0	125 (OWL)
Outerscale of turbulence	L_0=25 m
Number of actuators	10^5
Pupil sampling (simulation)	0.15 m/pixel
Correction frequency	1 Khz
Global Tip-Tilt correction	0.5 mas rms
Wavelength	2.2 μm
Bandpass	0.4 μm (in 9 channels)
Average Strehl ratio @ 2.2 μm	60%
Number of speckles realizations	1024

Table 1: Phase screens properties

4.1 The case of the single pupil: OWL

We present here the simulation results for the confusion problem in the case of an Extremely Large Telescope. We have chosen OWL for our study (Dierickx, these proceedings) because this is the extreme example for this type of achitecture and because the project is already technically quite advanced. We show in Figure 5 the shape of the pupil and the turbulence pattern after AO correction. Figure 6 presents the image of the polychromatic PSF affected by wavefront errors in the full K band and its averaged profile.

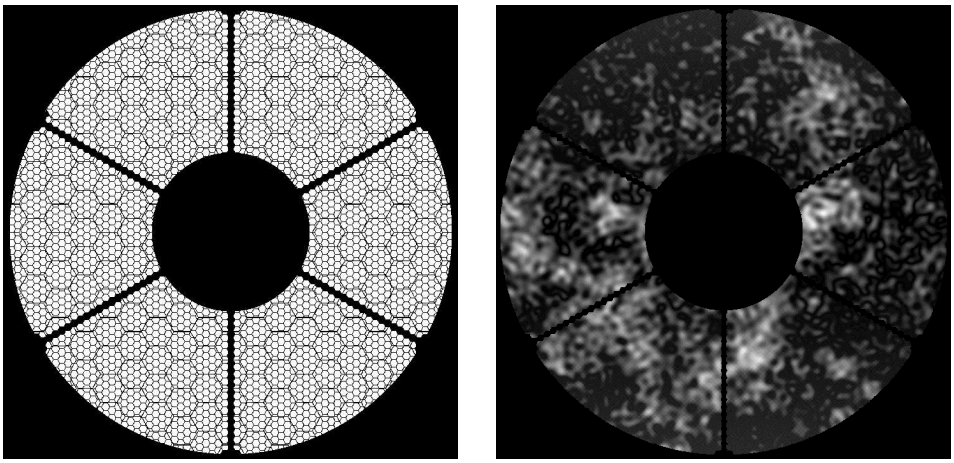

Figure 5: OWL pupil and OWL turbulence simulation. Left: full achitecture of the OWL pupil. Right: an example of corrected turbulence pattern generated with a PSD.

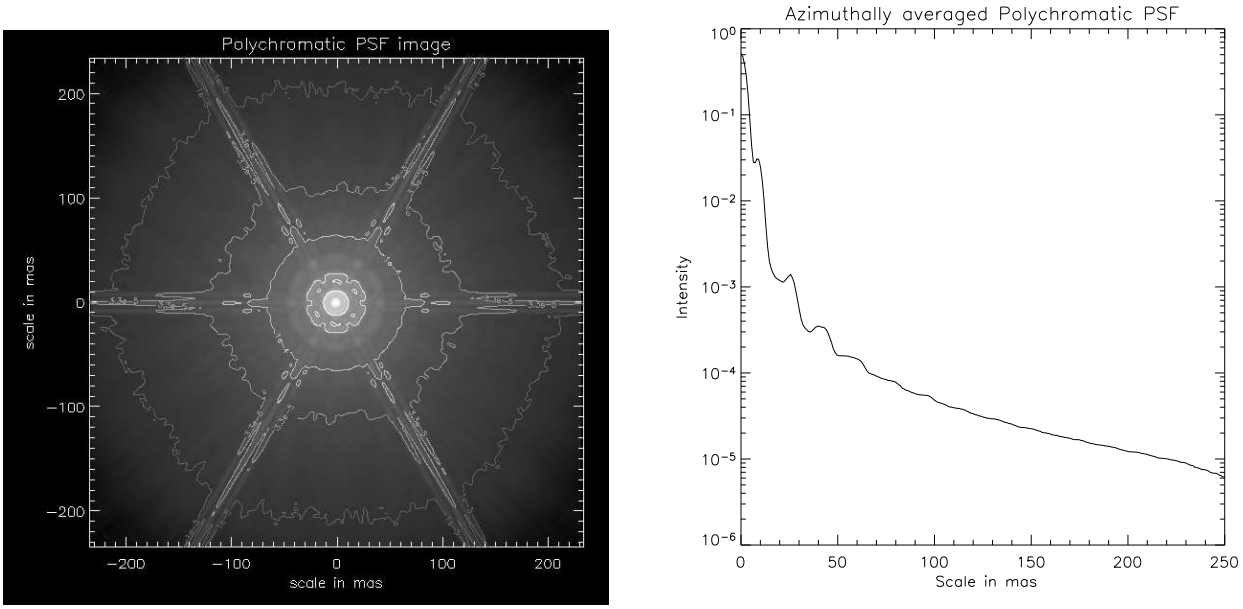

Figure 6: Polychromatic OWL PSF in the full K band affected by turbulence. Left: image of the PSF (the x and y scale in mas). Five contours are overplotted for the levels: 10^{-5}, 3.3×10^{-5}, 10^{-4}, 10^{-3} and 10^{-2}. The brightness scale is logarithmic. Right: azimuthally averaged profile of the PSF (x scale in mas).

4.2 The case of the interferometer

We simulate here the two different modes of interferometry: the Fizeau and densified modes. We will not discuss the IRAN mode here because its field of view is limited by the shape of the pupil. The corrected turbulence parameters are the same as previously assumed for OWL. Table 2 lists the properties of the interferometer. We have chosen a baseline of 100 meters to provide the same angular resolution as OWL.

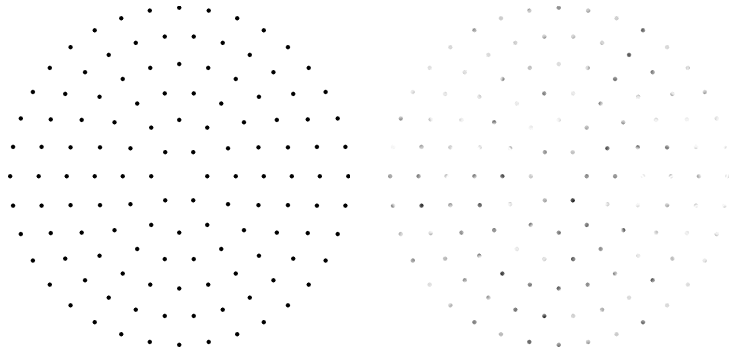

Figure 7: Interferometer pupil and turbulence simulation. Left: full achitecture of our interferometer. Right: an example of corrected turbulence pattern generated from a PSD.

Two different scientific programs can be carried out with interferometers: first, very large baseline interferometry with a relatively small number of sub-apertures (around 12 and 1 to 10 km baseline), which is useful for studying individual stars, circumstellar disks, exoplanets, or brown dwarfs [4], and secondly interferometry with a large number of sub-apertures (in our

[4]those objects requires only a little field of view (3×3 to 10×10 resels)

Number of sub-apertures	126
Baseline	100 m
Dilution factor	83.333
Number of rings	6
Sub-apertures diameter	1.2 m
Collecting surface	142.5 m^2
Surface ratio OWL/interferometer	41.8

Table 2: Interferometer properties

example, 126 telescopes) using smaller baselines (typically from 100 m to 1 km). This implementation, optimized for a larger field of view (395 resels in the snapshot image), opens the possibility to study more complex or fainter objects such as high redshift galaxies ($Z \approx 1-5$) or globular clusters around nearby galaxies.
The number of sub-apertures (126) may appear important, but it is much smaller than the 3500 hexagons of the OWL primary mirror. The interferometer is highly extensible: one can start with few telescopes (first ring) and then add sub-apertures (the following rings) to increase the limiting magnitude and the field of view.

We will simulate the Fizeau mode and the densified mode. In these two cases, we calculate the Fizeau PSF of the interferometer. The PSF considered here is just the polychromatic Fourier Transform of the sub-pupils. The Fizeau image will be simulated directly as a single pupil by direct convolution between astrophysical objects and PSF. We will take into account the effect of the smaller collecting surface of the interferometer on the limiting magnitude with an adequate coefficient factor. This configuration creates a large number of dispersed peaks with only one white peak at the true position of each object. The intensity of the secondary peaks decreases very slowly due to the sub-aperture PSF modulation (here $\theta > 1$" with 1.2 m of aperture diameter). This will obviously lied to confusion problems (see Figure 8).
Our simulation of the PSF uses a larger Strehl ratio (around 80%) than the first simulation with OWL, because on each sub-aperture, we obtain a best correction of piston and tip-tilt residues and the others modes contribute with a small weight.

We limit ourselves here to direct imaging without Earth rotation synthesis to cover the (u,v) plane.We will now consider multiple fields in densified configuration. Let us notice that all sub-apertures have the same shape (circular) and can be increased homothetically by densifying the pupil (Labeyrie 1996, Riaud et al. 2001, Gillet et al. 2003). As we already saw previously, we will get only one white peak with the full energy, but in a narrow field of view (ZOF), see Figure 9. We propose here to use an array of ZOF to cover the scientific field. In terms of calculation, this mode corresponds to the previous Fizeau image simulation multiplied by an appropriate Airy pattern that defines each field of view.

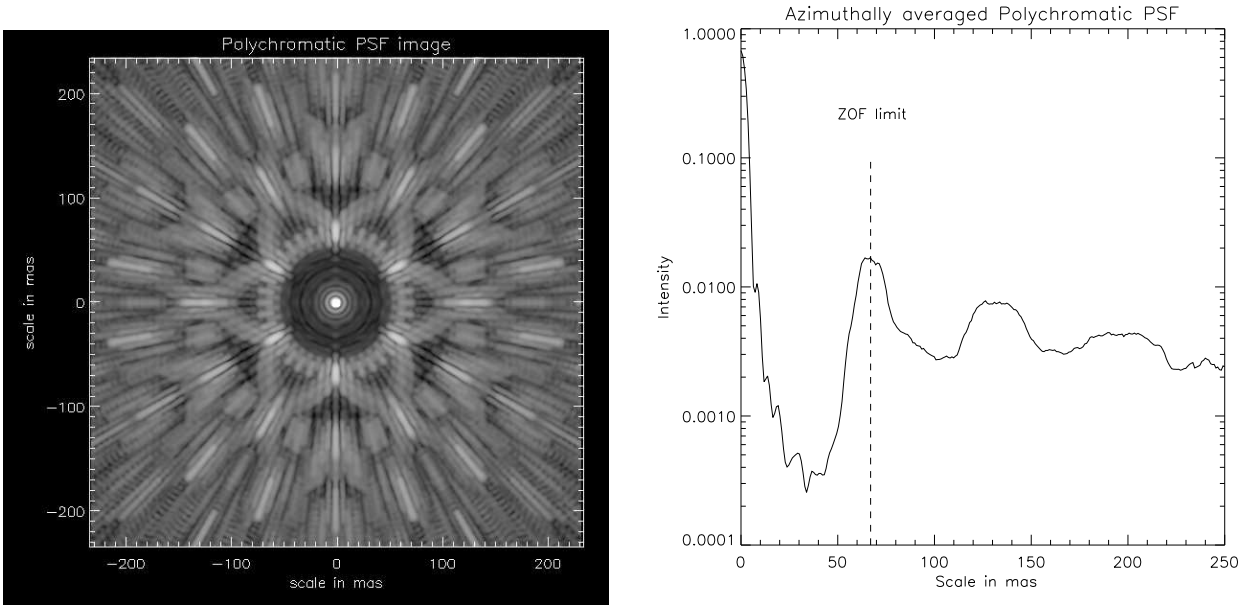

Figure 8: Polychromatic Fizeau PSF in the full K band. Left: image of the PSF (x and y scales in mas). The brightness scale is logarithmic. Right: azimuthally averaged profile of the PSF (x scale in mas). The limit of the ZOF is also shown.

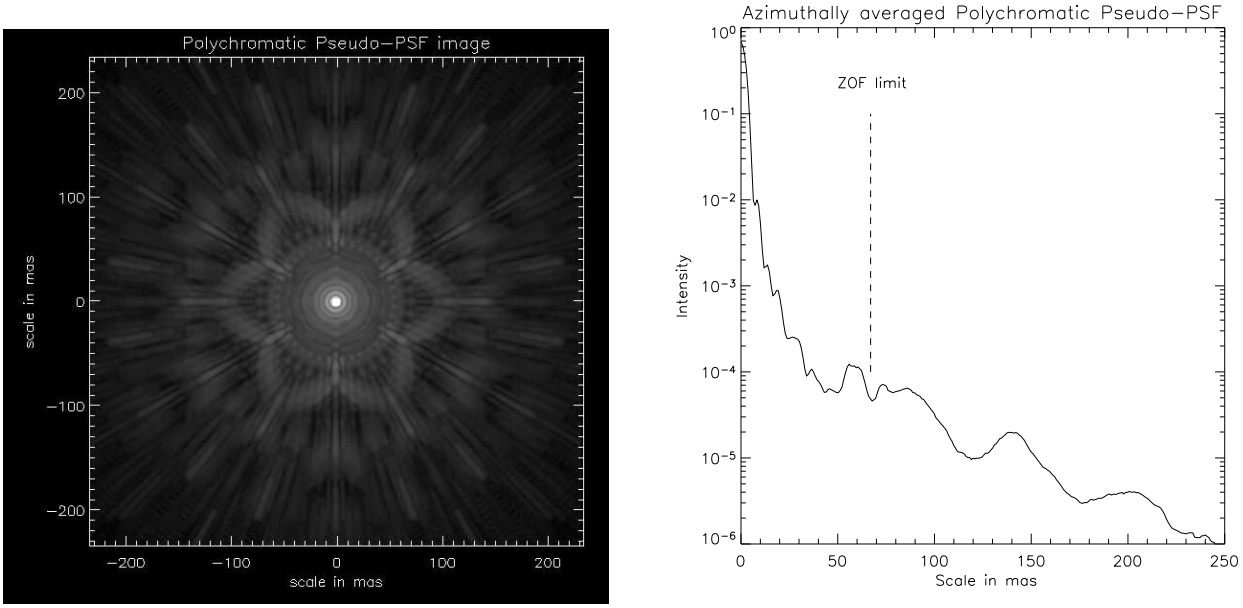

Figure 9: Polychromatic densified pseudo-PSF in the full K band. Left: image of the PSF (x and y scales in mas). The brightness scale is logarithmic. Right: azimuthally averaged profile of the PSF (x scale in mas).

5 Expected sky results with such architectures

After the Point Spread Function simulations for all configurations, we will compute in this chapter the expected loss in detectivity for one scientific example: a simulated field of highly redshifted galaxies (JWST/NIRCAM team).

A good choice of a crowded field of view with high dynamic objects is the case of highly redshifted galaxies. Indeed, our field of view presents a dynamic of 12 magnitudes between faint galaxies and bright foreground galaxies. We can explore precisely the effect of PSF contamination of bright objects on the fainter ones. It is also possible to add field stars to determine their effect. The simulations have been performed with large arrays (4096×4096) corresponding to a 4" $\times$ 4" total field of view. The input data given by the JWST/NIRCAM team was $2' \times 2'$ but due to the increased angular resolution of our architectures using 100 m baselines, we have decreased this input field of view in proportion.

We calculate the observed image for OWL and the Fizeau interferometer in two steps: first, we convoluate the input image with the previously calculated PSF and secondly, we apply photon noise and readout noise (15 e^-/pixel/frame) on the image obtained after convolution. The

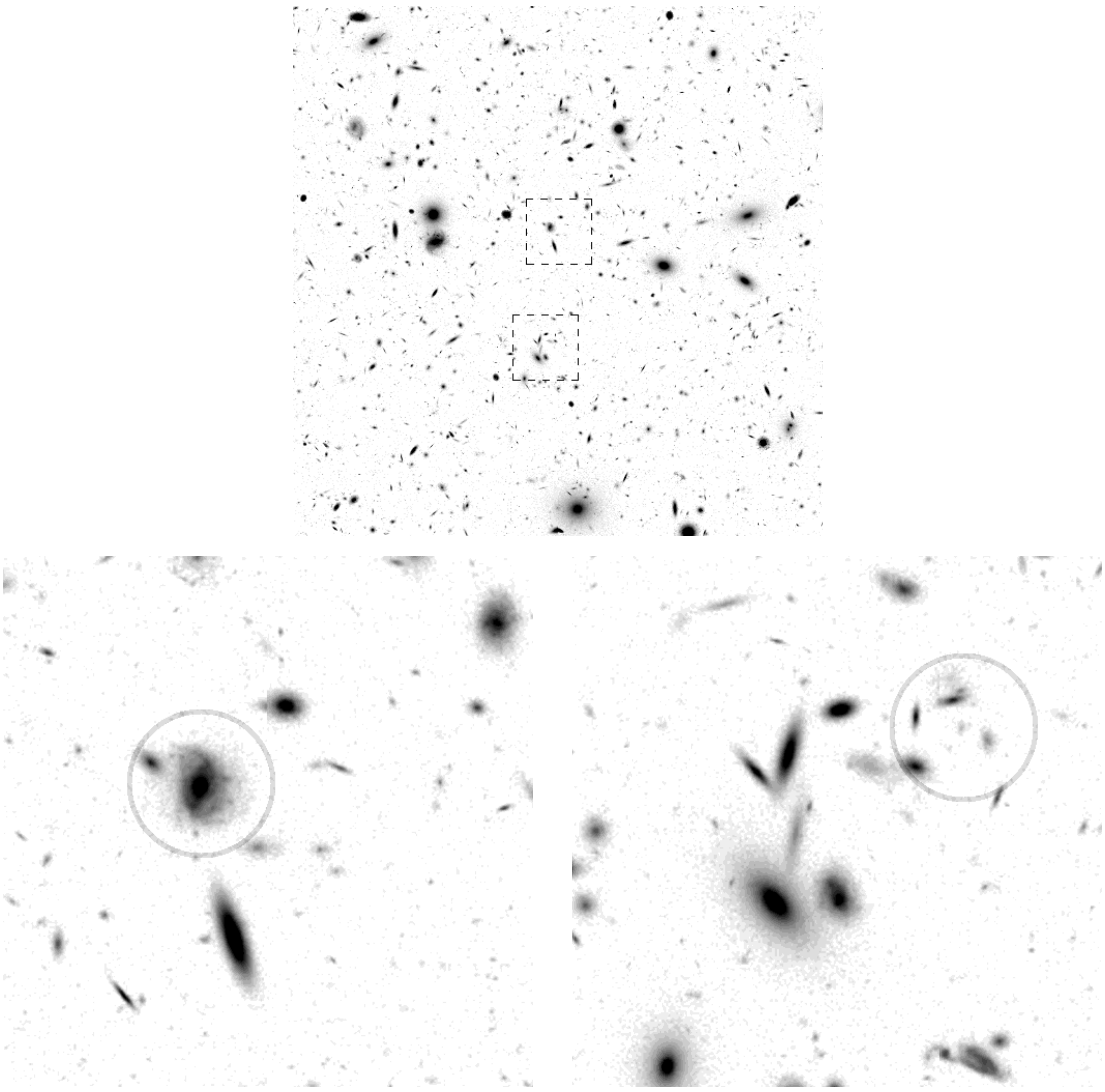

Figure 10: A simulated field of view of highly redshifted galaxies in the K band. Top: the full field of view (4096×4096 pixels or 4" $\times$ 4").The limiting magnitude is around 30 in the K band. For our simulations we decreased the original field of view size ($2' \times 2'$) by a factor 30. The two squares are the two different fields of view chosen to compare the detectivity of OWL with the Fizeau interferometer (enlarging in the two bottom figures). The two circles are the densified fields of view explored as examples. For lisibility all images are in negative brigthness scale.

detector is limited to 10^5 e^-/pixel due to saturation, so that we apply N times these two noises for the N individual exposures. The densified image simulation is slightly different: we proceed in the same way as in the Fizeau case for the convolution process, and then multiply the two observed fields of view by a polychromatic Airy pattern due to the densification process on the sub-apertures in the relayed pupil plane. The densified image can be seen as an observation through a port-hole (the polychromatic Airy pattern that delimits the ZOF). The interference function shape change according to its position in the ZOF.

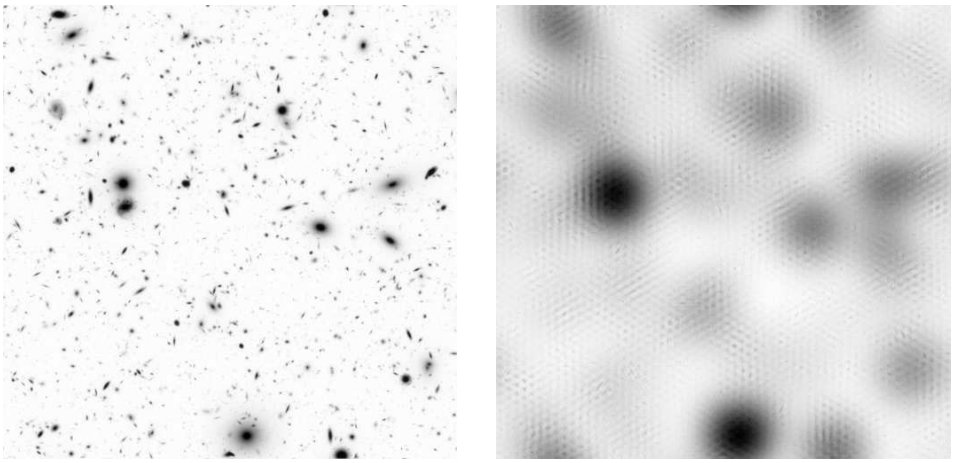

Figure 11: Left: The convolved field of view with the OWL PSF. The overall aspect remains similar to the target (see Fig. 10 top), but a fine analysis shows a loss of 3 magnitudes in sensitivity for the faintest objects. Right: The convolution with the Fizeau PSF shows a large confusion effect due to the extension of this one.

As expected, OWL presents the smallest loss. But the PSF has extended wings up to 200 mas in radus at the 10^{-5} level (see Fig. 6a), and the faintest sources are hidden in this halo. The loss is already 3 magnitudes in detectivity (see Fig. 11a and 12a, 12b) .
The case of Fizeau is more complicated. We first have a detectivity loss of 4 magnitudes due to the smaller collecting surface (142.5 m^2 compared to about 5950 m^2). In the Fizeau mode, most of the energy is in dispersed peaks: for example in our configuration only 1.6% of the energy is in the central resel, inducing a loss of 4.5 magnitudes. But the detectivity also depends on the distance between the reference source and a bright object: the loss is only 2 magnitudes when the bright source is in the ZOF (angular separation lower than 50 mas in radus) or outside the HOF (angular separation greater than 0.46 arcsec in radus), but the intermediate case presents a larger loss with a maximum of 3.5 magnitudes. The total loss is thus 10.5 to 12 magnitudes including PSF spreading, collecting surface and confusion noise (see Fig. 11b and 13a, 13b), to be compared with the loss of 3 magnitudes for OWL.

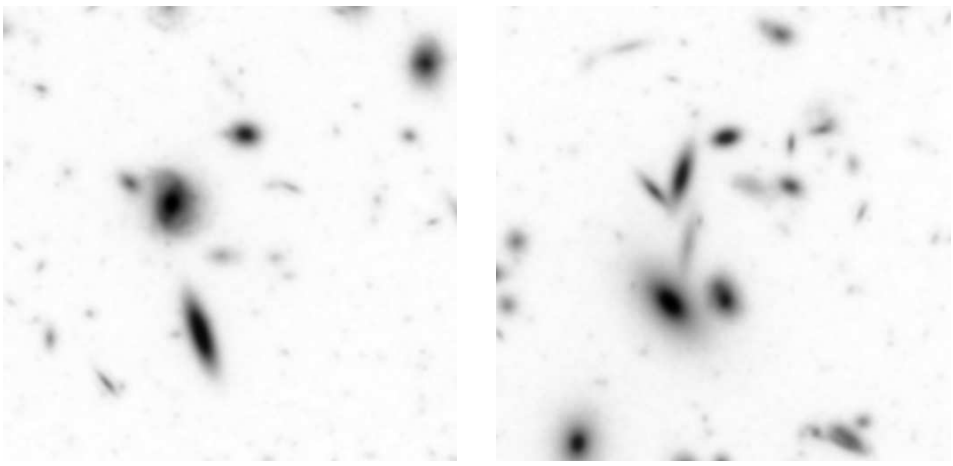

Figure 12: Simulation results for the two chosen sub-fields, in the case of OWL. The PSF convolution produces a small loss, but increases the level of background in a significant way compared with Figure 10b and 10c. The brightness scale is linear.

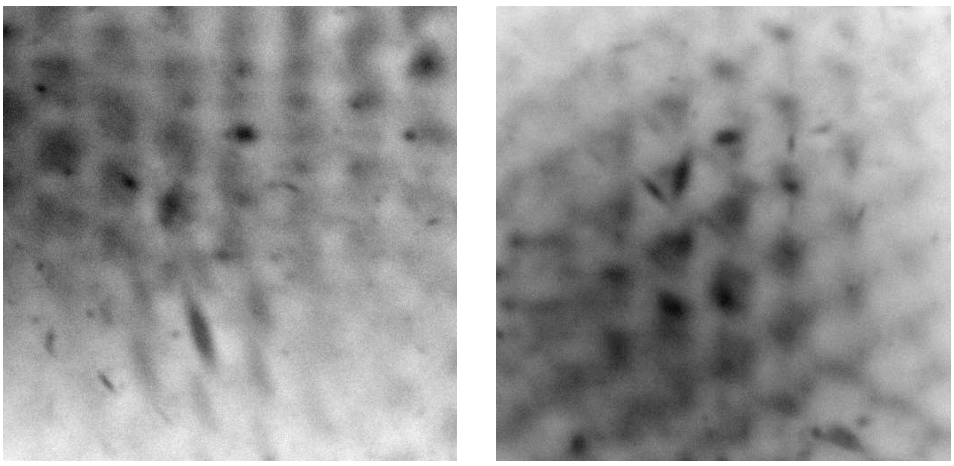

Figure 13: Same fields of view as Fig 12 seen through the Fizeau interferometer. The field shows an important crowding effect due to the high luminosity of the brightest galaxies located within and nearby the field of view. We clearly see the foregound galaxies replica due to the dispersed peaks increasing both the background level and the photon noise.

The simulation of densified snapshot imaging is rather close to Fizeau simulations and the gain compared to this one only comes from the enhancement of energy in the central resel. In our configuration, the central resel contains 27% of the total flux, yielding a gain of 3 magnitudes compared to the Fizeau mode (see Figure 14). The total loss thus decreases to about 8 magnitudes.

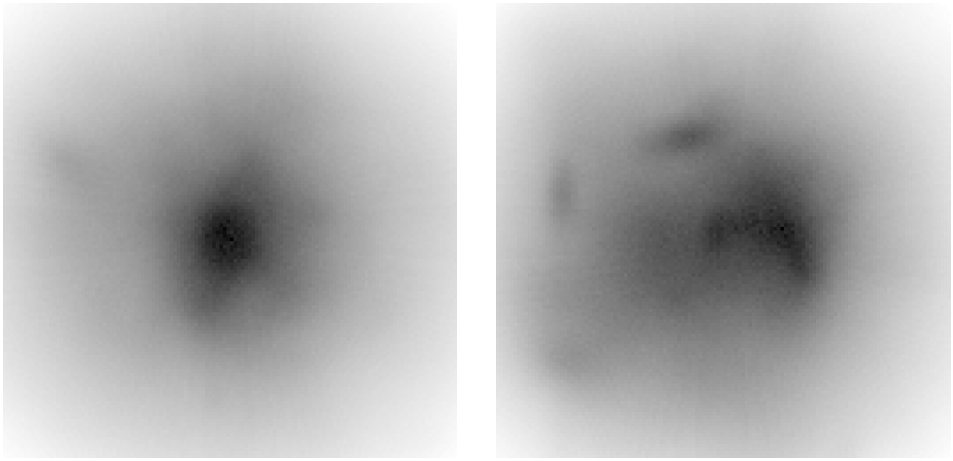

Figure 14: Enlarged image of the densified zero order field of view chosen in our two samples (see Fig.10b,c). The crowding effect due to the nearest bright sources is similar in the Fizeau image, but the densification procedure provides a gain on the photon noise, thanks to the intensification of central white peak.

6 Conclusions

We have reviewed the diffraction theory for single pupils and for imaging stellar interferometers, emphasizing on the concepts of the interferometric recombination techniques. When the collecting surface becomes important, the main limitation comes from confusion in the field of view. Indeed, a field of view may appear empty with a 8 m class telescopes, but with a 100 m-class like OWL this field contains many objects: faint stars, high redshifted galaxies.
We have first simulated the impulse response of the optical instruments with high order adaptive optics technology. Secondly, we have calculated the loss in detectivity for a sample object: a deep field with galaxies like the Hubble Deep Field or Ultra Deep Field. The case of OWL presents the smallest loss in detectivity compared to interferometric architectures, but it is not negligible with 3 magnitudes and potential problems with foreground bright stars ($m_k < 18$) near the galactic plane. For this last problem, it is possible to use multiple Lyot coronagraphs (Lyot 1939) such as implemented in the VIMOS instrument with multiple slits to limitate the diffraction effect of stars.
The second result is interesting because it appears that interferometric architectures with a large number of small sub-apertures can provide sufficient image quality for a crowded field of view. Moreover, the use of densification technique increases by 3 magnitudes the limiting magnitude of classical Fizeau interferometers. Interferometry therefore seems to be useful not only for stellar objects but also for more complex objects like galaxies. This study did not take into account the gain for all interferometric cases associated to aperture synthesis or post-processing data analysis. Finally, the technical development of ion etching ultra-light mirrors could provide an important cost reduction and open possibilities to build such imaging interferometer in the next twenty years.

References

Fizeau H., 1868, CR. Acad. Sci. Paris,t , 68,932
Gillet S. et al. 2003, A&A 400, 393
Guyon O., 2003, A&A 404, 379
Labeyrie A. , 1996, A&AS, 118, 517
Lyot B. 1939, MNRAS, 99, 580
Michelson A.A & Pease F.G, 1921, Aj, 53, 249
Riaud P. et al., 2001, 36th Liège Int. Astroph. Coll., 85
Roddier F., 1987, Progress in Optics 19, 281
Roddier F. & Ridgway S.T., 1999, PASP, 111, 990
Vakili & al., 2004, A&A 421, 147